Published in IET Microwaves, Antennas & Propagation
Received on 23rd August 2010
Revised on 7th June 2011
doi: 10.1049/iet-map.2010.0413

ISSN 1751-8725

Design of the current driver for inducing radiating ground edge current in a printed circuit board

T.-I. Liu Y.-S. Wang S.-J. Chung

Department of Communication Engineering, National Chiao Tung University, Hsinchu, Taiwan
E-mail: sjchung@cm.nctu.edu.tw

Abstract: A new current driver is proposed to effectively excite ground edge current for radiation without additional space reserved for antenna design. Since the current driver functions as a feeding structure as opposed to a radiator, it can be designed as small as possible without deteriorating the antenna radiation properties. A circuit model of the miniaturised balun (balanced to unbalanced transformer) is introduced to explain the current-inducing mechanism and to provide some valuable physical insights into the characteristics of the current driver. The effect of a shielding metal box for the proximity circuitry near the current driver is also investigated. And it is shown that the nearby shielding box has minor effect on the performance of the driver, which demonstrates the feasibility of the current driver as an effective antenna structure in a compact wireless terminal. The current driver operating at 2.45 GHz is printed on an FR4 substrate of 0.4 mm and occupies only a small area of about 4 mm by 4 mm. The simulated and measured results come to a great agreement. Nearly omni-directional radiation patterns with a peak gain of about 1 dBi are obtained. Owing to the design flexibilities and the compactness, the current driver is feasible for wireless applications.

1 Introduction

Owing to the demand of compact devices in many wireless applications, most of the circuit board area is filled with radio frequency (RF) and baseband circuitry, and there is a very limited space reserved for the antenna. Thus, many miniaturisation techniques have been proposed so as to integrate the antenna in the restricted small circuit board area. However, it is challenging to scale down the antenna size while maintaining good antenna properties. The subject of antenna miniaturisation has been extensively investigated in various literatures. As has been shown in [1–3], some techniques applied to the substrate were utilised for antenna size reduction including the magneto-dielectric composite substrate and the embedded-circuit metasubstrate. However, the cost of the fabrication of these substrates is quite high, so they are not practical for real applications. Electrically small antennas (ESAs) are easy to be integrated into the circuit, but the external matching circuit are required because of the highly reactive impedance of the ESAs. Although the aforementioned drawbacks can be circumvented by placing a parasitic element near the ESAs to achieve resonance and impedance matching simultaneously in a small area to approach the theoretically lower bound of the quality factor Q [4, 5], the bandwidth is still limited by the overall size. Planar inverted-F antennas (PIFAs) are popular because of the great degree of design flexibility to multiband and compactness. The PIFA antenna with a spiraling tail or a capacitive loading is capable of dual-band operation with about 50% size of the conventional one [6]. In [7–10], the composite right/left-handed transmission line can also be used to design the compact resonant antennas.

The above-mentioned antenna miniaturisation techniques mostly focus on the geometry modification. However, antenna size has fundamental limitations with consideration about gain, bandwidth and efficiency [11–13]. To achieve better antenna properties, the finite ground plane on the printed circuit board (PCB) has to be considered in the antenna design process. In [14], the performance of the mobile phone for GSM 900/1800 operation was analysed by the combination of two coupled resonators: the antenna and the chassis (finite length ground plane). The results indicated that the chassis is dominant in contribution of radiation in a lower-frequency band. With the increasing knowing of the finite ground plane, there are various techniques applied to the ground plane for better antenna performance, such as cutting slots [14, 15], using wave traps [16] and adding ground edge current choke [17]. To date, we have known that the ground plane can be used for antenna design, but the challenge is how to effectively utilise the ground plane for radiation. Some attempts that utilise the ground plane as the main radiator were published. Coupler-element-based antenna designs can excite the chassis resonant mode so that the whole ground plane can radiate effectively [18, 19]. Nevertheless, the position, size and shape of the coupler are restricted for achieving appropriate capacitive coupling. Also, they are still bulky because of the need of the matching circuit. Traditional quarter wavelength slot antennas cut on the ground edge, or their miniaturised versions, are easy to induce radiating edge current. However, these slot antennas

are still responsible for partial radiation so the size reduction is limited even with the capacitive loading or external matching circuit employed [20–22].

In this paper, a new current driver as shown in Fig. 1 is proposed to activate the ground current flowing along the circuit board edge for radiation. The essential concept is to exploit the ground plane as a main radiator. The current driver mainly works to transform the input RF signal into the ground edge current and has little responsibility for radiation. Therefore the current driver can be designed as small as possible without the necessity to consider much about the degradation of antenna radiation performance. The idea underlying the design of the current driver is to divide the ground plane into two parts so that the RF signal can be fed in between the parts, without being short circuited, to excite the radiating edge currents. This idea was actually realised in the previous investigations. As shown in [23], the ground plane is physically separated so that the ground plane can be fed as a thick dipole antenna with appropriate feeding network to achieve impedance matching. However, physical separation of the ground plane is impractical for many applications. In the present study, the ground plane is electrically separated by the proposed compact current driver, which is composed of a very small slot at the edge, a short coupling strip and a lumped capacitor connected in between the slot. The overall size of the current driver is only $3\% \times 3\%$ of the space wavelength. Without the need of the additional matching circuit, the current driver is matched by coupling the RF signal to the ground edge through broadside coupling. The equivalent circuit model for the current driver is regarded as a miniaturised planar balun with the differential ports connected to the ground edge [24]. Thus, the ground edge current behaves similar to a dipole antenna fed by the miniaturised balun. The main radiator is the ground plane as opposed to the current driver so the size of the driver can be very small while maintaining good radiation properties.

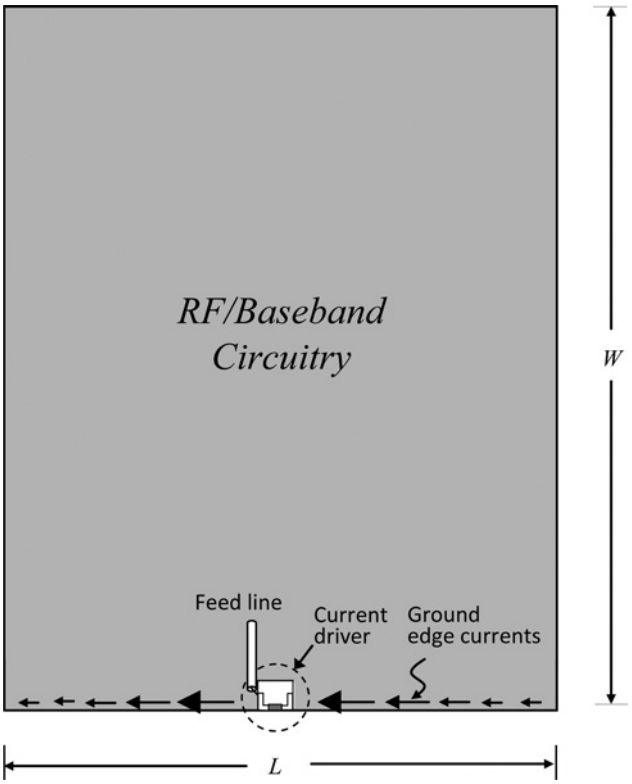

Fig. 1 *Schematic diagram for the antenna concept*
Most of the PCB is occupied by RF and/or baseband circuitry (grey area)

This paper is organised as follows. Section 2 describes the geometry and equivalent circuit model of the current driver. Section 3 presents the design of the current driver with structure parameter and ground size study. The influence of a metal box for shielding the nearby circuitry is discussed in Section 4. Section 5 shows the measured results with some discussions. Finally, Section 6 gives a brief conclusion.

2 Geometry and circuit model

The proposed current driver is demonstrated at 2.45 GHz for IEEE 802.11 b/g/n WLAN applications. It is fabricated on the ground edge of an FR4 substrate with thickness $h = 0.4$ mm and dielectric constant $\varepsilon_r = 4.4$. The size of the substrate is $L \times W = 50$ mm $\times$ 100 mm, which is the standard size for Personal Computer Memory Card International Association (PCMCIA) applications.

As shown in Fig. 1, the current driver should be able to generate differential output currents flowing along the circuit board edge so that in-phase radiation in the far field can be obtained. This implies that the current driver fed by a coaxial line or microstrip line should perform a circuit function like a balun with the differential ports connected to the ground edge. Figs. 2*a* and *b* show the perspective view and top view of the proposed current driver, respectively. The letters in the figure designate the relative position in the

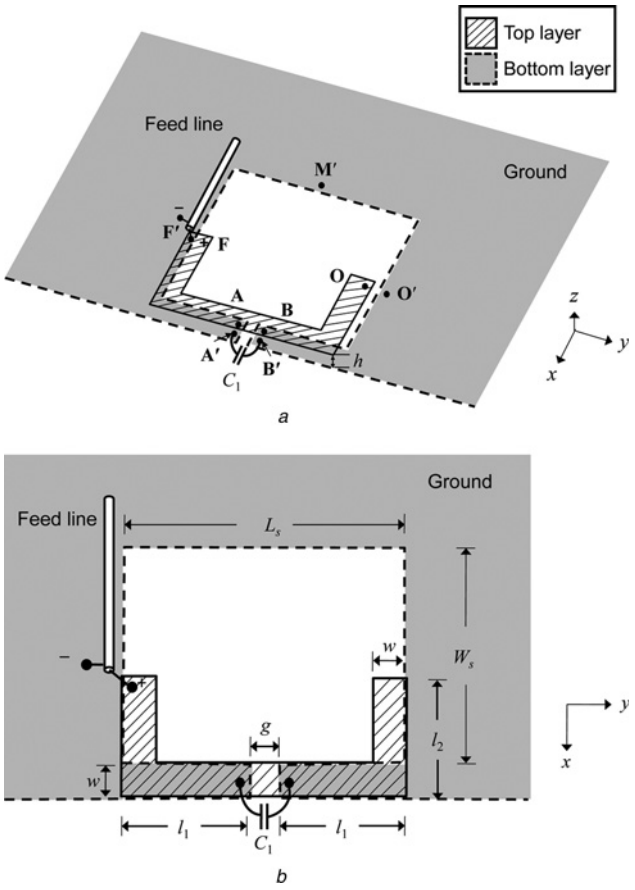

Fig. 2 *Prospective view and configuration of the proposed current driver*

a Perspective view of the proposed current driver, where F, A, B and O points are on the top layer, and F′, A′, B′, O′ and M′ points are on the bottom layer

b Configuration of the proposed current driver

doi: 10.1049/iet-map.2010.0413

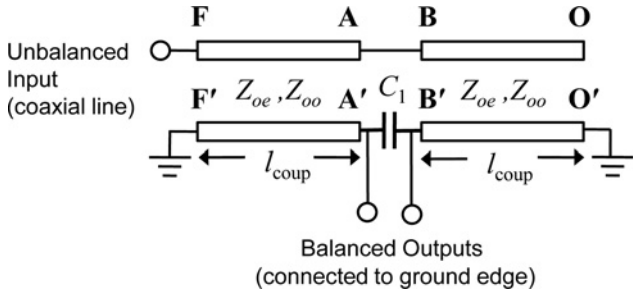

Fig. 3 *Equivalent circuit for the proposed current driver*

equivalent circuit model shown in Fig. 3. The current driver lies in the *xy* plane and is printed on both sides of the FR4 substrate. It comprises a U-shaped metal strip with strip width of w on the top layer and a slot of size $L_s \times W_s$ on the bottom layer. The slot is open to the ground edge through a small gap g. A lumped-circuit capacitor C_1 is connected in between points A′ and B′ on the bottom layer. This capacitor here can also be replaced by a printed one. The current driver is fed by a 50 Ω feed line, which can be a coaxial line or a microstrip line. The positive terminal of the feed line is connected to one end of the U-shaped strip (point F) on the top layer, and the negative terminal is connected to the ground point near the slot edge (point F′) on the bottom layer. The overall size of the current driver is only 4 mm × 4 mm, which is about $0.03\lambda_0 \times 0.03\lambda_0$, with λ_0 being the free-space wavelength at 2.45 GHz.

To explain the operating principle of the current driver, an equivalent circuit model is introduced. It has to be emphasised that this equivalent circuit model is a conceptual model, but not an exact one. In spite of that, the circuit model gives a valuable understanding of the properties of the current driver.

The circuit model is derived as follows: in Fig. 2*a*, it is noted that the U-shaped metal strip couples to the overlapping slot edge mostly through broadside coupling. Here, a section from points F to A (top layer) and that from F′ and A′ (bottom layer) are considered as a pair of coupled lines. These two coupling transmission lines share the same ground $\overline{F'M'O'}$ along the slot edge on the bottom layer. The reason as to why they form two coupled lines but not a single transmission line will become clear when the simulated surface current distribution on them are depicted later. Similarly, the parallel sections $\overline{BO}$ (top layer) and $\overline{B'O'}$ (bottom layer) form another pair of coupled lines with the same ground $\overline{F'M'O'}$. The equivalent circuit model can thus be drawn as Fig. 3, which is actually a miniaturised planar balun similar to a conventional planar marchand balun [25, 26], but with difference in the capacitor C_1 between the balanced outputs (points A′and B′) for size reduction [24]. As the current driver has a function like a balun, it can generate differential signals at the two ends of the capacitor so the in-phase ground edge currents could be induced. The total radiation is mainly attributed to these induced ground edge currents.

The miniaturised planar balun with a lumped-circuit capacitor shows more degrees of freedom in design than the conventional planar marchand balun does. It can be implemented by a wide range of practical values for even-mode impedance Z_{0e} and odd-mode impedance Z_{0o} depending on various values of C_1 with different lengths of coupled lines. Moreover, this miniaturised balun structure is theoretically perfect and frequency independent with amplitude and phase balances. Several important characteristics of the miniaturised planar balun that are beneficial to the design of the current driver are listed in the following:

1. The required value of Z_{0e} for the balun increases with decreasing coupled line length l_{coup}.
2. The required value of Z_{0e} for the balun decreases when the capacitance C_1 increases.
3. The required value of Z_{0o} is not sensitive to the coupled line length or the capacitance C_1.
4. For a fixed coupled line length, the balun with larger Z_{0e} and smaller C_1 exhibits a wider bandwidth.

From characteristics (1) and (2), it shows that the balun size can be reduced with large C_1 whereas Z_{0e} remains fixed. However, characteristic (4) indicates the balun with larger Z_{0e} exhibits wider bandwidth, so C_1 and Z_{0e} are appropriately chosen depending on the desired bandwidth.

The proposed current driver is designed in a similar way like the miniaturised balun. The even-mode impedance Z_{0e} of the current driver is determined by the slot width W_s, which is related to the equivalent distance between coupled lines and ground plane. Thus, Z_{0e} increases with a larger slot width W_s. The coupling strength between the coupled lines is affected by the strip width w, so odd-mode impedance Z_{0o} is related to the strip width w. A larger strip width w corresponds to a lower value of the odd-mode impedance. Also, as stated in (4), the bandwidth increases when Z_{0e} increases, and thus the larger slot size for the current driver. Therefore bandwidth and size are trade-offs.

3 Design

As stated, the current driver is characterised by the even-mode impedance Z_{0e}, the odd-mode impedance Z_{0o}, the length of the coupled lines l_{coup} and the capacitor in the circuit model. In this section, the current driver is investigated through the simulated results of the return loss and total gains on the z-axis for these parameters. The simulation results are obtained using an Ansoft High-Frequency Structure Simulator (HFSS) [27]. The FR4 substrate loss is considered in the simulation with the loss tangent of 0.02.

Fig. 4 shows the simulated return loss and gains on the z-axis for the current driver with various capacitances C_1. It is observed that the centre frequency is shifted downwards

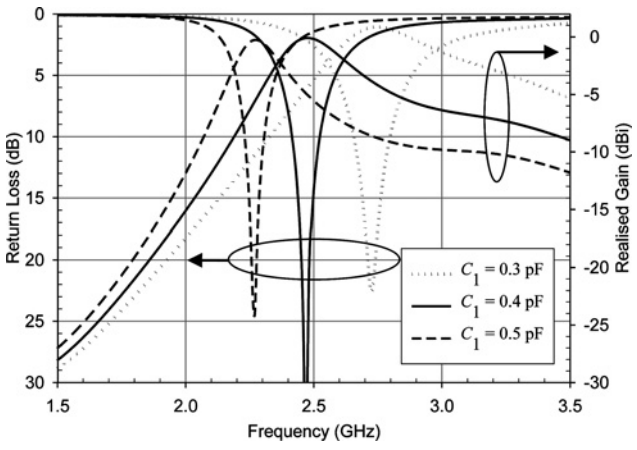

Fig. 4 *Simulated return loss and total gains on the z-axis for the proposed current driver as a function of C_1*

Other structure parameters are given as follows: $L_s = 4$ mm, $W_s = 3.5$ mm, $l_1 = 1.5$ mm, $l_2 = 2$ mm, $w = 0.5$ mm, $g = 1$ mm

with increasing C_1, from 2.73 to 2.27 GHz as C_1 varies from 0.3 to 0.5 pF. This trend of the return loss agrees with characteristics (1) and (2) of the miniaturised balun, which indicate that the capacitor C_1 is used for size reduction. Good impedance matching is also maintained with various C_1, so the centre frequency of the current driver can be easily adjusted by varying C_1 with little influence on impedance matching. Furthermore, the peak gain on the z-axis keeps a value near 0 dBi, not changed much because of the variation of C_1. The variations of gain over the 10 dB impedance bandwidth of the current driver for $C_1 = 0.3$, 0.4 and 0.5 pF are 0.66, 0.5 and 0.4 dBi, respectively. This suggests that the ground edge current induced by the current driver maintains good radiation property despite the change of C_1, and thus the centre frequency.

The slot width W_s is a crucial parameter related to the even-mode impedance of the coupled lines in the equivalent model. Characteristic (1) of the miniaturised balun shows the required value of Z_{0e} increases with decreasing coupled line length. Thus, the operating frequency moves downwards when the slot width W_s increases. Fig. 5 illustrates the simulated return loss and gains on the z-axis with W_s equal to 3, 3.5 and 4 mm. As seen in the figure, the centre frequency is shifted downwards from 2.59 to 2.36 GHz as the slot width W_s increases from 3 to 4 mm. In the meanwhile, the peak gain at the centre frequency remains nearly unchanged. It is worth noting that both C_1 and W_s can be used to adjust the operating frequency of the current driver with negligible effect on the impedance matching.

Here, the coupled lines are bent into two sections l_1 and l_2 for size reduction. The effect of the length of coupled lines is examined by adjusting l_1 whereas l_2 is fixed to 1.5 mm. Fig. 6 depicts the return loss and gains on the z-axis for various strip length l_1 (1, 1.5 and 2 mm). Obviously, the centre frequency moves lower with larger l_1. As l_1 increases from 1 to 2 mm, the centre frequency decreases from 2.78 to 2.22 GHz. Note that the peak gain on the z-axis for various l_1 is quite stable.

Fig. 7 shows the effect on return loss and gains on the z-axis for various strip width w (0.3, 0.5 and 0.8 mm). There is a slight frequency shift shown in the figure with varying w. The strip width is related to the coupling coefficient of the coupled lines, especially in the l_1 section. In addition, the strip width has a dominant effect on Z_{0o} but

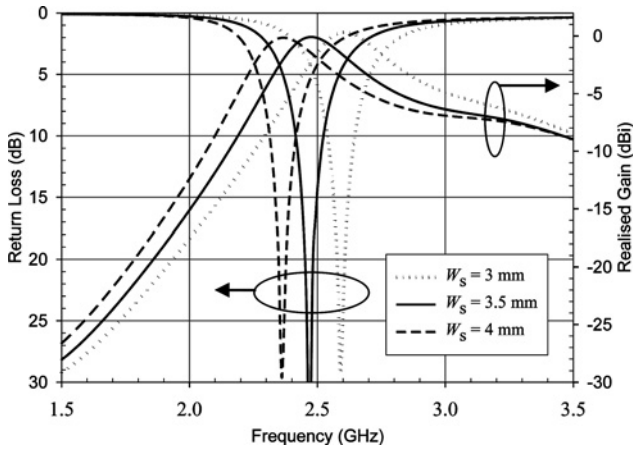

Fig. 5 *Simulated return loss and total gains on the z-axis for the proposed current driver as a function of slot width, W_s*

Other structure parameters are the same as those given in Fig. 4 with $C_1 = 0.4$ pF

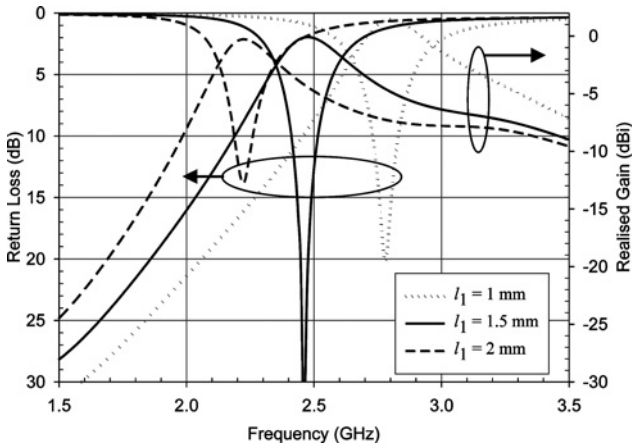

Fig. 6 *Simulated return loss and total gains on the z-axis for the proposed current driver as a function of l_1*

It is noted here that slot length L_s varies with l_1 ($L_s = 2l_1 + g$). Other structure parameters are the same as those given in Fig. 4 with $C_1 = 0.4$ pF

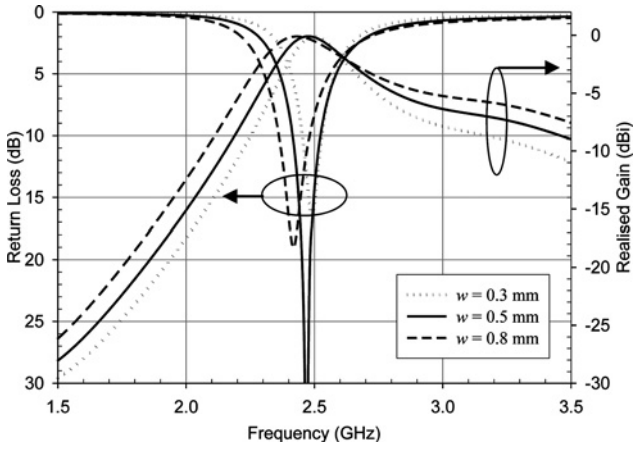

Fig. 7 *Simulated return loss and total gains on the z-axis for the proposed current driver as a function of strip width, w*

Other structure parameters are the same as those given in Fig. 4 with $C_1 = 0.4$ pF

a subtle effect on Z_{0e}. Since the required value of Z_{0o} is less sensitive to the coupled line length (characteristic 3). Thus, the change of strip width w would not lead to a large frequency shift as expected.

According to characteristic (4) of the miniaturised balun mentioned earlier, the balun with larger Z_{0e} and smaller C_1 exhibits wider bandwidth. This property is illustrated in Fig. 8, which shows the return loss and gains on the z-axis for two sets of C_1 and the corresponding slot width W_s ($C_1 = 0.4$ pF, $W_s = 3.5$ mm and $C_1 = 0.2$ pF, $W_s = 6$ mm). The 10 dB return loss bandwidth changes from 120 MHz (2.40 to 2.52 GHz) to 230 MHz (2.33 to 2.56 GHz) as C_1 varies from 0.4 pF ($W_s = 3.5$ mm) to 0.2 pF ($W_s = 6$ mm). The cost of bandwidth enhancement for the current driver is a larger slot size. Thus, the current driver can be designed flexibly for various requirements of bandwidth. In this study, the current driver is designed for 2.45 GHz IEEE 802.11 b/g/n WLAN applications. The bandwidth of the current driver with $C_1 = 0.4$ pF and $W_s = 3.5$ mm is adequate for the specification.

After the discussion on the effects of the structure parameters and the capacitor C_1 on the current driver, it is necessary to

doi: 10.1049/iet-map.2010.0413

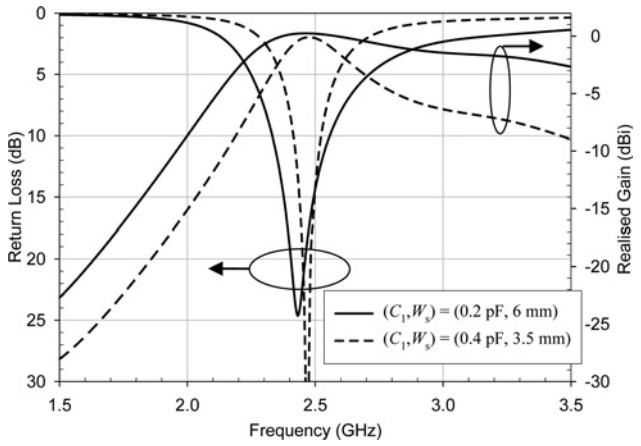

Fig. 8 *Simulated return loss and total gains on the z-axis for the proposed current driver with two configurations ($C_1 = 0.2$ pF, $W_s = 6$ mm) and ($C_1 = 0.4$ pF, $W_s = 3.5$ mm)*

Other structure parameters of the current driver ($C_1 = 0.2$ pF, $W_s = 6$ mm) are $L_s = 4$ mm, $l_1 = 1.5$ mm, $l_2 = 3$ mm and $w = 0.5$ mm. The structure parameters of the current driver ($C_1 = 0.4$ pF, $W_s = 3.5$ mm) are the same as shown in Fig. 4

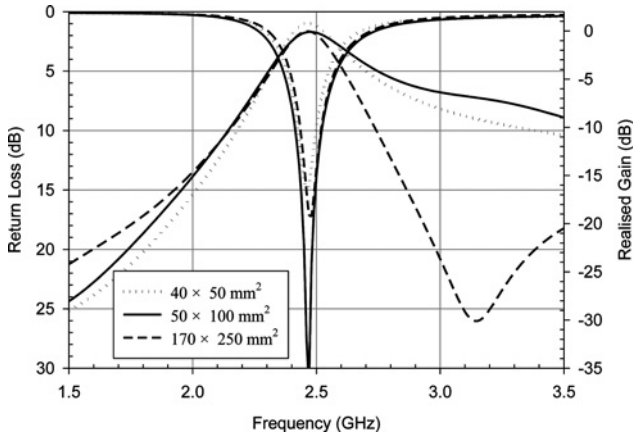

Fig. 9 *Simulated return loss and total gains on the z-axis for the proposed current driver with ground sizes $L \times W = 40 \times 50$ mm^2, 50×100 mm^2 and 170×250 mm^2*

Current driver is placed in the centre of the ground edge L. Structure parameters for the current driver are the same as shown in Fig. 4 with C_1=0.4 pF

investigate the sensitivity of the antenna performance to ground size. Fig. 9 shows that the return loss for various ground sizes, $L \times W = 40 \times 50$ mm^2, 50×100 mm^2 and 170×250 mm^2. It is seen that the ground size has minor effect on the return loss for the current driver. The centre frequency is almost unchanged with different ground sizes. The gains on the z-axis are also shown in the figure. As observed, the peak gains and gain variations in the 10 dB return-loss bandwidth are about the same. The rapid gain variation in the higher outband for the ground size of 170×250 mm^2 is because of the high-order-mode current distribution along the edge.

4 Shielding box effect

As shown previously, the design trend of the hand-held devices is compactness for better mobility. However, in addition to the antenna miniaturisation, electromagnetic interference (EMI) is also important when all devices are fabricated on a small circuit board. It is common to address EMI problems by covering the RF circuitry with a shielding metal box to isolate it from the interference. Owing to the skin effect, the outside current cannot penetrate into the inside of the shielding box. Although there are openings on the shielding box for the signals to come in and out, the shielding box still functions well because the size of the openings is very small compared to the wavelength of the operating frequency.

The effect of the shielding box on the current driver is investigated. As shown in Fig. 10, the shielding box is placed on the top layer with surrounding shorting points connected to the ground plane through the substrate. The geometrical parameters of the shielding box are length l_{box}, width w_{box} and height h_{box} ($+z$ direction). The distance between the shielding box and the current driver is decomposed into two components, vertical component d_x and horizontal component d_y. Fig. 11 helps to understand the effect of the shielding box on the return loss and gains of the current driver when the shielding box is placed at different positions. The size of the shielding box is $l_{box} \times w_{box} \times h_{box} = 20 \times 20 \times 2$ mm^3. As seen in Fig. 11*a*, the frequency responses of the return loss have similar behaviours for $d_x = 3$, 1 and 0 mm (with d_y fixed at 0 mm). The centre frequency is slightly shifted from 2.48 to 2.63 GHz. The more the shielding box is moved towards the current driver, the higher is the centre frequency. Only 6% frequency shift is observed even when the shielding box is put directly above the current driver (i.e. $d_x = d_y = 0$ mm). As will be seen later, this slight frequency shift can be easily restored by tuning the driver's structure parameter. Although not shown here, the shielding box has a negligible effect on the current driver when the vertical distance is more than 3 mm. Also, since the induced current is concentrated on the ground edge for radiation, the effect of the shielding box

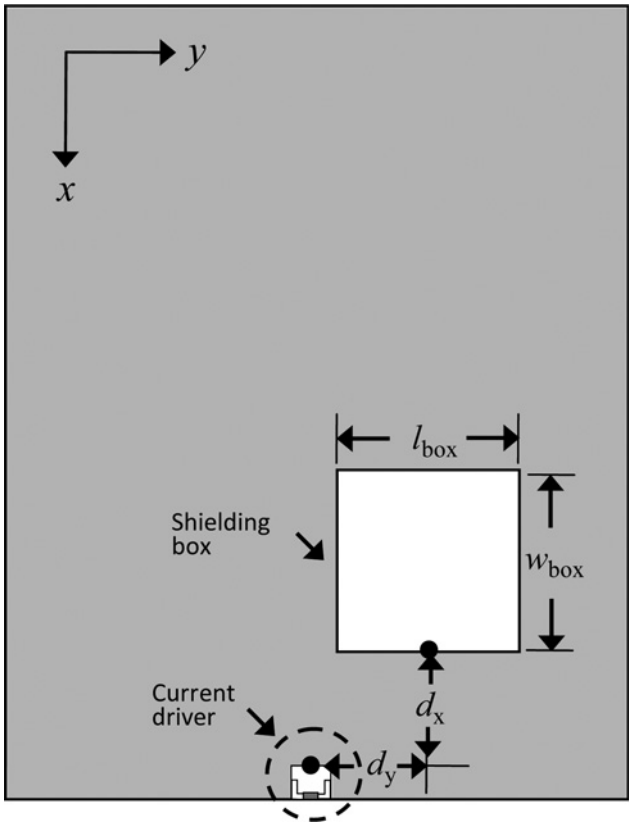

Fig. 10 *Configuration of the current driver and the shielding box*

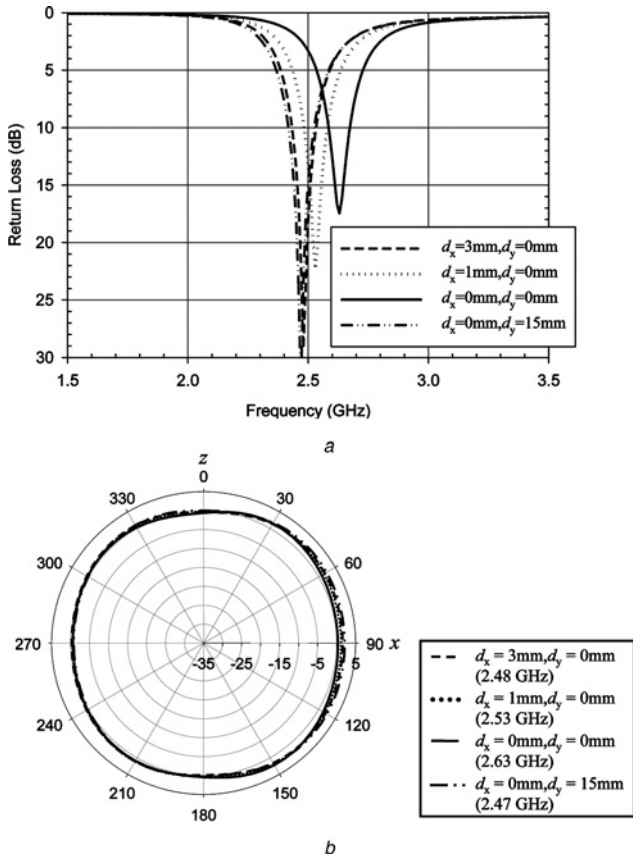

Fig. 11 *Simulated return loss and simulated total radiation field patterns for the current driver*

a Simulated return loss for the proposed current driver with the shielding box of different positions

b Simulated total radiation field patterns in *xz* plane for the current driver with shielding box of different positions. The size of the shielding box is $20 \times 20 \times 2$ mm^3. The structure parameters of the current driver are the same as shown in Fig. 4 with $C_1 = 0.4$ pF

placed along the edge is also considered. The fourth curve in Fig. 11*a*, $d_x = 0$ mm and $d_y = 15$ mm, represents the return loss when the shielding box is aligned with the right side of the ground edge. The response is almost identical to that of a stand-alone current driver, which means that the proximity shielding box has no obvious effect on the current driver.

Fig. 11*b* shows the simulated total radiation field patterns in *xz* plane for the current driver with the shielding box at different positions. The radiation patterns are omni-directional and almost the same with average gains varying between 0.65 and 1.04 dBi. This implies that the existence of the nearby shielding box has little influence both on the return loss response and the radiation performance of the current driver.

The influence of the shielding box volume is examined in Fig. 12, which shows the return loss of the current driver for various sizes of the shielding box. It can be seen that the return loss is nearly not affected by the width and height of the shielding box. The return loss curve for the 20 mm × 20 mm × 2 mm shielding box is almost overlapped with the curve for the 40 mm × 40 mm × 2 mm one. Furthermore, by comparing the first curve (20 mm × 20 mm × 2 mm) and the second curve (20 mm × 20 mm × 4 mm), the centre frequency moves from 2.63 to 2.65 GHz as h_{box} varies from 2 to 4 mm. This variation shows that the height of the shielding box has minor effect on the return loss.

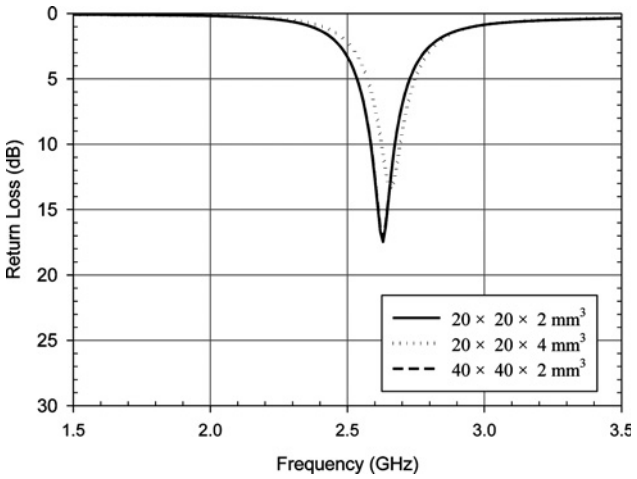

Fig. 12 *Simulated return loss for the proposed current driver with shielding box of different sizes*

Shielding box is aligned with the slot edge of the current driver ($d_x = 0$ mm and $d_y = 0$ mm). The structure parameters of the current driver are the same as shown in Fig. 4 with $C_1 = 0.4$ pF

From the above discussion, the vertical distance d_x of the shielding box is the most important factor that determines the amount of frequency shift. However, even in the worst case where the shielding box is placed directly above the current driver (i.e. $d_x = d_y = 0$ mm), the frequency shift can be easily resumed by slightly adjusting the current driver's dimension. To demonstrate this, Fig. 13 shows the simulated return loss with and without the presence of a shielding box. The dotted line indicates the frequency response of the original design (with slot size of $L_s \times W_s = 4 \times 3.5$ mm^2) without the proximity shielding box, which shows a design frequency at 2.47 GHz. After putting the shielding box of size 20 mm × 20 mm × 2 mm directly above the current driver ($d_x = d = 0$ mm), the response turns out to be the dashed line, where the centre frequency is now shifted to 2.63 GHz. To tune the frequency into the design one, we simply increase the slot width W_s of the current driver from 3.5 to 4.2 mm. The increase of the slot width would decrease the centre frequency (as shown in Fig. 5), so that the resultant frequency response (solid line) resumes to the design one.

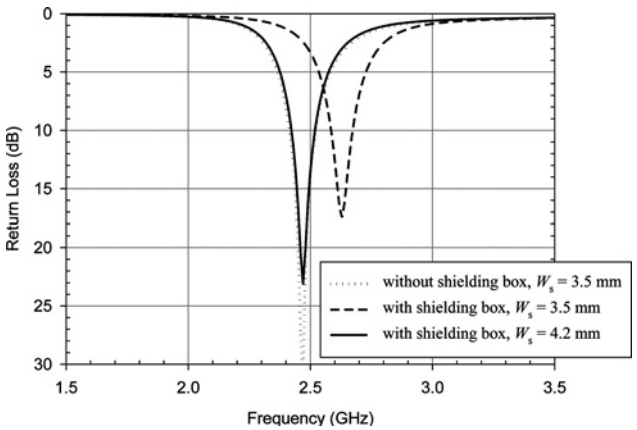

Fig. 13 *Simulated return loss for the proposed current driver with and without the presence of the shielding box*

Shielding box is placed directly above the current driver ($d_x = 0$ mm and $d_y = 0$ mm) with the size of $20 \times 20 \times 2$ mm^3. Other structure parameters are the same as those given in Fig. 4 with $C_1 = 0.4$ pF

doi: 10.1049/iet-map.2010.0413

5 Measurements and discussion

Fig. 14 shows the simulated return loss and radiation efficiency as well as the measured return loss for the proposed current driver with a ground plane of size $L \times W = 50\ \text{mm} \times 100\ \text{mm}$. The simulated and measured return loss comes to a great agreement. The measured centre frequency is 2.46 GHz with a 10 dB return-loss bandwidth of about 120 MHz. In addition, over the bandwidth for 2.4 GHz WLAN operation, the radiation efficiency varies from 74 to 86%, which is no worse than the radiation efficiency of general miniaturised antennas.

Fig. 15 illustrates the measured radiation patterns at 2.45 GHz in the three principal planes. There are generally no nulls for the total-power radiation pattern E_{total} in the three principal planes. This omni-directional property makes the proposed current driver promising for many applications. The corresponding values of measured peak and average gains in three principal planes are listed in Table 1. The simulated average gain for the nearly omni-directional pattern in xz plane is about 1 dBi. The gain difference between the simulated and measured results is because of the ohmic loss caused by the cable and the lumped capacitor. The radiation properties of the current driver are quite good, as compared to general printed antennas fabricated on the same substrate.

To further understand the radiation mechanism, Fig. 16 shows the simulated surface current distribution for the current driver at 2.45 GHz. One can observe that the radiating ground edge currents induced by the current driver can be decomposed into two parts: the out-of-phase x-direction currents and the in-phase y-direction currents. Note that the out-of-phase x-direction currents spaced by near half-wavelength in free space produce maximum radiation fields in $\pm y$ directions but null fields in $\pm z$ directions. Thus, a digit '8' radiation pattern for the E_φ component is obtained in the yz plane as shown in Fig. 15c. In the xz plane, the inverted x-direction currents cancel each other in the far field, so the radiation pattern for the E_θ component is small. Moreover, the in-phase y-direction currents are responsible for the omni-directional radiation patterns for the E_φ component in the xz plane and form a digit '8' radiation pattern for the E_θ component in the yz plane. The current distribution is consistent with the measured radiation pattern shown in Fig. 15. This implies

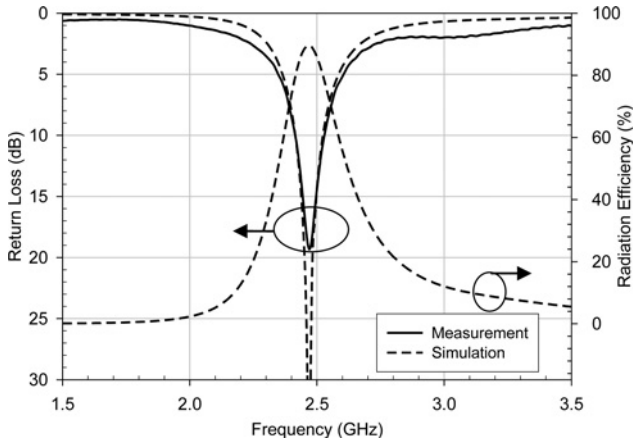

Fig. 14 *Simulated return loss and radiation efficiency as well as measured return loss for the proposed current driver connected with a ground plane of 50 mm × 100 mm*

Simulated radiation efficiency includes the mismatch loss. Structure parameters for the current driver are the same as shown in Fig. 4 with C_1=0.4 pF

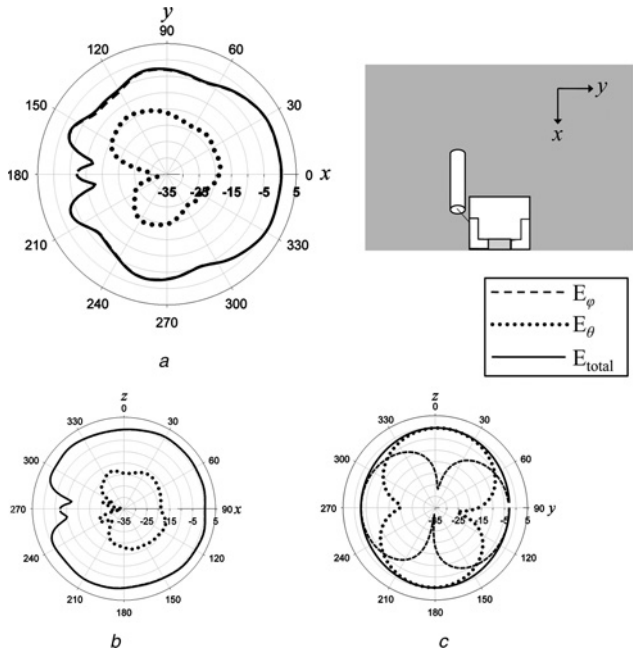

Fig. 15 *Measured 2-D radiation patterns for the proposed current driver at 2.45 GHz with a connected ground of 50 mm by 100 mm*

a xy plane
b xz plane
c yz plane

Table 1 Measured gains at 2.45 GHz

Measured gain, dBi	xy plane	xz plane	yz plane
peak gain	0.44	1.20	−0.36
average gain	−2.65	−0.07	−1.67

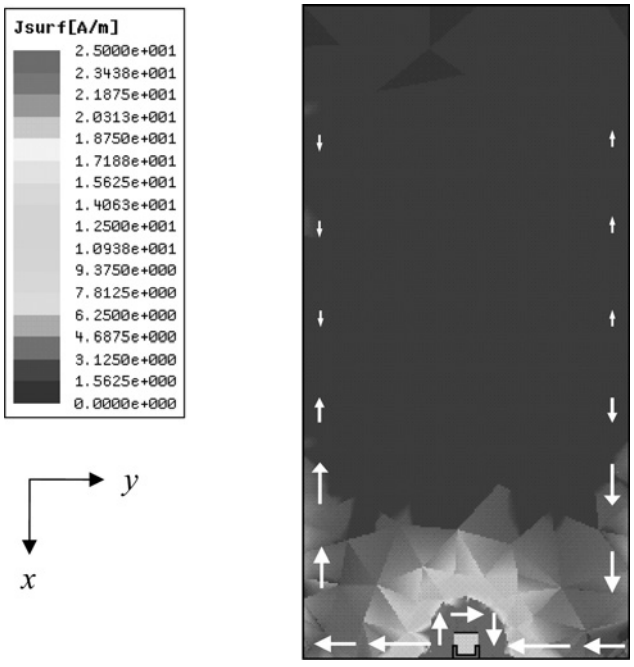

Fig. 16 *Simulated surface current distribution for the proposed current driver at 2.45 GHz*

that the main radiation source comes from the current along the ground edge.

To further understand the radiation mechanism, Fig. 16 shows the simulated surface current distribution for the current driver at 2.45 GHz. One can observe that the radiating ground edge currents induced by the current driver can be decomposed into two parts: the out-of-phase x-direction currents and the in-phase y-direction currents. Note that the out-of-phase x-direction currents spaced by near half-wavelength in free space produce maximum radiation fields in $\pm y$ directions but null fields in $\pm z$ directions. Thus, a digit '8' radiation pattern for the E_φ component is obtained in the yz plane as shown in Fig. 15*c*. In the xz plane, the inverted x-direction currents cancel each other in the far field, so the radiation pattern for the E_θ component is small. Moreover, the in-phase y-direction currents are responsible for the omni-directional radiation patterns for the E_φ component in the xz plane and form a digit '8' radiation pattern for the E_θ component in the yz plane. The current distribution is consistent with the measured radiation pattern shown in Fig. 15. This implies that the main radiation source comes from the current along the ground edge.

The close view of the surface current distribution in the current driver is depicted in Fig. 17. Although there are strong currents concentrated in the structure, the currents have little contribution to radiation since the size of the current driver is far smaller than the ground plane. In addition, the radiation from the current on the current driver cancels each other in the far field. Therefore it shows again that the main radiation is contributed by the ground edge current. As mentioned in Section 2, the parallel sections $\overline{FA}$ and $\overline{F'A'}$ form coupled lines instead of a single transmission line. This can be verified from the current distribution illustrated in Fig. 17, which shows that the currents on the two parallel sections flow in the same direction. It is also true for the currents on the parallel

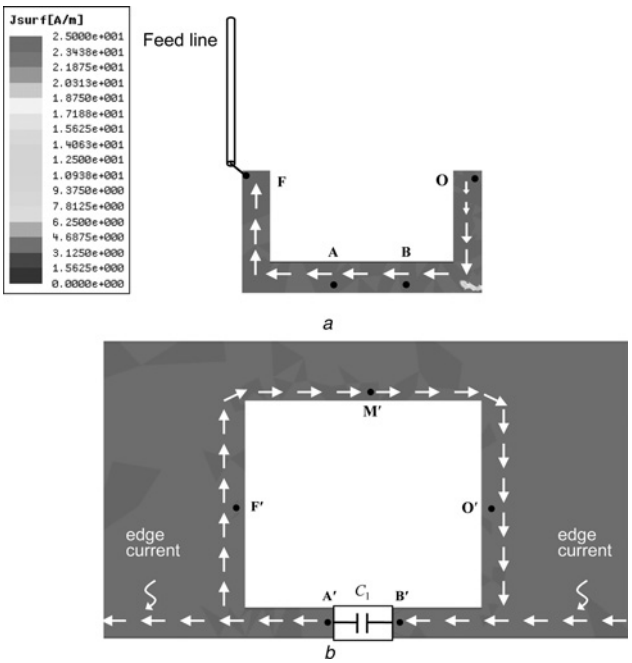

Fig. 17 *Close view of the simulated current distribution for the proposed current driver at 2.45 GHz*

a Top view
b Bottom view

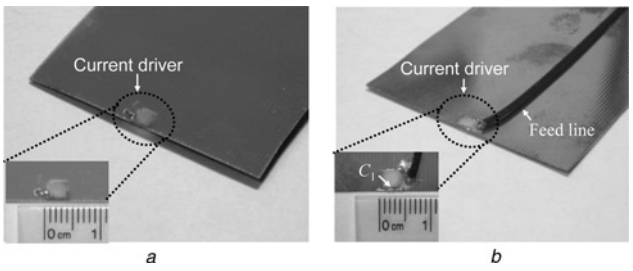

Fig. 18 *Photograph of the fabrication for the proposed current driver with a connected ground plane of 50 mm × 100 mm*

a Top view
b Bottom view

section $\overline{BO}$ and $\overline{B'O'}$. The photograph of the fabricated current driver is shown in Fig. 18.

6 Conclusions

In this paper, a novel antenna concept that utilises a current driver to activate the ground edge current for radiation is proposed. The main point is that the main radiator is the ground plane as opposed to the current driver. The current driver operates like a small feeding structure with little contribution to radiation, so the current driver could be designed very small while good radiation properties are maintained. The current driver is investigated through the equivalent circuit model, which is viewed as a miniaturised planar balun. Thus, the in-phase ground edge currents can be induced for radiation. The results of the parameter study for the current driver are consistent with the characteristics of the miniaturised balun. The performance of the current driver is insensitive to the ground size. The centre frequency is nearly unchanged with different ground sizes. This suggests that the current driver can be easily applied to various applications. Also, the influence of the shielding box is thoroughly investigated. It shows that the effect of the shielding box on the current driver is minor even when the box is placed very close to the current driver. The good radiation properties are achieved with simulated radiation efficiency over 74%. Near omni-directional radiation patterns with the peak gain of about 1 dBi are obtained for the current driver of size about $0.03\lambda_0 \times 0.03\lambda_0$ (λ_0 is the free-space wavelength at 2.45 GHz). The experimental results agreed well with the simulation.

The current driver has advantages of compact size and ease of fabrication. Thus, it could be easily applied to laptops, mobile phones and other communication devices. Compared to the conventional miniaturised antennas, the current driver is more competitive in commercial applications. In addition to the ground plane, the current driver could also be integrated into the metal packages. It provides a wide variety of applications for the current driver. Related research is being undertaken now.

7 References

1 Mosallaei, H., Sarabandi, K.: 'Magneto-dielectrics in electromagnetic: concept and applications', *IEEE Trans. Antennas Propag.*, 2004, **52**, (6), pp. 1558–1567
2 Buell, K., Mosallaei, H., Sarabandi, K.: 'A substrate for small patch antennas providing tunable in miniaturization factors', *IEEE Trans. Microw. Theory Tech.*, 2006, **54**, (1), pp. 135–146
3 Mosallaei, H., Sarabandi, K.: 'Design and modeling of patch antenna printed on magneto-dielectric embedded-circuit metasubstrate', *IEEE Trans. Antennas Propag.*, 2007, **55**, (1), pp. 45–52

doi: 10.1049/iet-map.2010.0413

4 Erentok, A., Ziolkowski, R.W.: 'Metamaterial-inspired efficient electrically small antennas', *IEEE Trans. Antennas Propag.*, 2008, **56**, (3), pp. 691–707
5 Jin, P., Ziolkowski, R.W.: 'Low-Q, electrically small, efficient near-field resonant parasitic antennas', *IEEE Trans. Antennas Propag.*, 2009, **57**, (9), pp. 2548–2563
6 Wang, Y.-S., Lee, M.-C., Chung, S.-J.: 'Two PIFA-related miniaturized dual-band antennas', *IEEE Trans. Antennas Propag.*, 2007, **55**, (3), pp. 805–811
7 Lee, C.-J., Leong, K.M.K.H., Itoh, T.: 'Composite right/left-handed transmission line based compact resonant antennas for RF module integration', *IEEE Trans. Antennas Propag.*, 2006, **54**, (8), pp. 2283–2291
8 Lee, J.-G., Lee, J.-H.: 'Zeroth order resonance loop antenna', *IEEE Trans. Antennas Propag.*, 2007, **55**, (3), pp. 994–997
9 Wang, Y.-S., Hsu, M.-F., Chung, S.-J.: 'A compact slot antenna utilizing a right/left-handed transmission line feed', *IEEE Trans Antennas Propag.*, 2008, **56**, (3), pp. 675–683
10 Pyo, S., Han, S.-M., Baik, J.-W., Kim, Y.-S.: 'A slot-loaded composite right/left-handed transmission line for a Zeroth-order resonant antenna with improved efficiency', *IEEE Trans. Microw. Theory Tech.*, 2009, **57**, (11), pp. 2775–2782
11 Hansen, R.C.: 'Fundamental limitations in antennas', *Proc. IEEE*, 1981, **69**, (2), pp. 170–182
12 Harrington, R.F.: 'Effect of antenna size on gain, bandwidth, and efficiency', *J. Res. Natl. Bur. Stand.*, 1960, **64D**, pp. 1–12
13 McLean, J.S.: 'A re-examination of the fundamental limits on the radiation Q of electrically small antennas', *IEEE Trans. Antennas Propag.*, 1996, **44**, (5), pp. 672–676
14 Vainikainen, P., Ollikainen, J., Kivekäs, O., Kelander, I.: 'Resonator-based analysis of the combination of mobile handset antenna and chassis', *IEEE Trans. Antennas Propag.*, 2002, **50**, (10), pp. 1433–1444
15 Hossa, R., Byndas, A., Bialkowski, M.E.: 'Improvement of compact terminal antenna performance by incorporating open-end slots in ground plane', *Microw. Opt. Technol. Lett.*, 2004, **14**, (6), pp. 283–285
16 Lindberg, P., Öjefors, E.: 'A bandwidth enhancement technique for mobile handset antennas using wavetraps', *IEEE Trans. Antennas Propag.*, 2006, **54**, (8), pp. 2226–2233
17 Wang, Y.-S., Lu, J.-C., Chung, S.-J.: 'A miniaturized ground edge current choke—design, measurement, and applications', *IEEE Trans. Antennas Propag.*, 2009, **57**, (5), pp. 1360–1366
18 Villanen, J., Ollikainen, J., Kivekäs, O., Vainikainen, P.: 'Coupling element based mobile terminal antenna structures', *IEEE Trans. Antennas Propag.*, 2006, **54**, (7), pp. 2142–2153
19 Huang, L., Russer, P.: 'Electrically tunable antenna design procedure for mobile applications', *IEEE Trans. Microw. Theory Tech.*, 2008, **56**, (12), pp. 2789–2797
20 Cabedo-Fabres, M., Antonino-Daviu, E., Valero-Nogueira, A., Ferrando-Bataller, M.: 'Wideband radiating ground plane with notches'. Proc. IEEE AP-S. Int. Symp. Digest, Washington, DC, USA, July 2005, pp. 560–563
21 Lindberg, P., Öjefors, E., Rydberg, A.: 'Wideband slot antenna for low-profile hand-held terminal applications'. Proc. 36th European Microwave Conf. 2006, Manchester, UK, September 2006, pp. 1698–1701
22 Li, C.-L., Chang, J.-P., Wong, L.-J.: 'Miniature planar notch antenna of J shape', *Electron. Lett.*, 2006, **42**, (20), pp. 1134–1135
23 Holopainen, J., Villianen, J., Valkonen, R., *et al.*: 'Mobile terminal antennas implemented using optimized direct feed'. IEEE Int. Workshop on Antenna Tech, iWAT 2009, Santa Monica, CA, USA, 2–4 March 2009
24 Ang, K.S., Leong, Y.C., Lee, C.H.: 'Analysis and design of miniaturized lumped-distributed impedance-transforming baluns', *IEEE Trans. Microw. Theory Tech.*, 2003, **51**, (3), pp. 1009–1017
25 Tsai, M.C.: 'A new compact wideband balun'. IEEE Microwave Millimeter-Wave Monolithic Circuits Symp. Digest, 1993, pp. 123–125
26 Maas, S.A., Chen, K.C.: 'A broad-band, planar, doubly balanced monolithic Ka-band diode mixer', *IEEE Trans. Microw. Theory Tech.*, 1993, **41**, (12), pp. 2330–2335
27 (HFSS-Ansoft Corporation: 'High frequency structure simulator (HFSS) version 10.0' (Ansoft Corporation, USA), 2007)